Bioelectromagnetics 41:175–187 (2020)

Effect of Pulsed Electromagnetic Fields on Human Mesenchymal Stem Cells Using 3D Magnetic Scaffolds

Alyaa I. Aldebs,[1] Fatema T. Zohora,[1] Nasim Nosoudi,[2] Surinder P. Singh,[3] and Jaime E. Ramirez-Vick[1]*

[1]*Department of Biomedical, Industrial & Human Factors Engineering, Wright State University, Dayton, Ohio*
[2]*Biomedical Engineering Program, Marshall University, Huntington, West Virginia*
[3]*CSIR-National Physical Laboratory, New Delhi, India*

Alternative bone regeneration strategies that do not rely on harvested tissue or exogenous growth factors are needed. One of the major challenges in tissue reconstruction is recreating the bone tissue microenvironment using the appropriate combination of cells, scaffold, and stimulation to direct differentiation. This study presents a bone regeneration formulation that involves the use of human adipose-derived mesenchymal stem cells (hASCs) and a three-dimensional (3D) hydrogel scaffold based on self-assembled RADA16 peptides containing superparamagnetic iron oxide nanoparticles (NPs). Although superparamagnetic NPs could be used as stimulus to manipulate the cell proliferation and differentiation, in this paper their use is explored for assisting osteogenic differentiation of hASCs in conjunction with direct stimulation by extremely low-frequency pulsed electromagnetic fields (pEMFs). Cellular morphology, proliferation, and viability, as well as alkaline phosphatase activity, calcium deposition, and osteogenic capacity were monitored for cells cultured up to 21 days in the 3D construct. The results show that the pEMFs and NPs do not have any negative effect on cell viability, but instead distinctly induced early differentiation of hASCs to an osteoblastic phenotype, when compared with cells without biophysical stimulation. This effect is attributed to synergy between the pEMFs and NPs, which may have stimulated mechanotransduction pathways, which, in turn activated biochemical signals between cells to differentiate or proliferate. This approach may offer a safe and effective option for the treatment of non-union bone fractures. Bioelectromagnetics. 2020;41: 175–187. © 2020 The Authors. *Bioelectromagnetics* published by Wiley Periodicals, Inc.

Keywords: 3D tissue constructs; electromagnetic stimulation; iron oxide nanoparticles; mesenchymal stem cells; magnetic scaffolds

INTRODUCTION

Bone fractures represent a substantial incidence and cost burden among musculoskeletal injuries in the United States, with 15.3 million cases each year, of which 5–10% involve complications such as delayed or non-unions [Yelin et al., 2016]. The development of alternative bone regeneration therapies for the treatment of bone fractures, which do not rely on harvested tissue or exogenous growth factors and cells, are critically needed. However, creating living tissue constructs that are structurally, functionally, and mechanically comparable to the natural bone has been a challenge [Polo-Corrales et al., 2014]. For instance, recreating the bone tissue microenvironment using the appropriate combination of cells, scaffold, and stimulation is needed to direct differentiation [Polo-Corrales et al., 2018]. Since approval by the U.S. Food and Drug Administration (FDA) almost four decades ago, low-frequency pulsed electromagnetic fields (pEMFs) have been widely used in orthopedics as an adjuvant therapy for the treatment of bone disorders to reduce healing complications [Lohmann et al., 2000]. In vitro, in vivo, and clinical studies have

Conflict of interest: None.

*Correspondence to: Jaime E. Ramirez-Vick, Department of Biomedical, Industrial & Human Factors Engineering, Wright State University, 3640 Colonel Glenn Highway, Dayton, OH 45435. E-mail: jaime.ramirez-vick@wright.edu

Received for review 30 October 2018; Accepted 1 January 2020

DOI:10.1002/bem.22248
Published online 15 January 2020 in Wiley Online Library (wileyonlinelibrary.com).

suggested the significant role of pEMF in the bone repair process [Daish et al., 2018]. Studies propose that the forced vibration of free ions present on the surface of a cellular plasma membrane under the influence of pEMF, regulates cell signaling processes and influences cell proliferation and differentiation [Panagopoulos et al., 2002; Markov, 2007; Ross et al., 2015; Ayala et al., 2018]. Many investigations have focused on the use of external stimuli to accelerate cell proliferation and osteogenic differentiation of progenitor cells, such as mesenchymal stem cells (MSCs).

A strategy to improve fracture healing is to understand the bone tissue microenvironment where mechanical stimuli are important and necessary for bone health and homeostasis [Voog and Jones, 2010]. This type of stimuli mediates an adaptive remodeling response in bone at the cellular level, through a process known as Wolff's law [Lanyon, 1974; Lanyon and Baggott, 1976; Woo et al., 1981]. At the molecular level, the cells transduce mechanical force-induced signals into biochemical responses through mechanotransduction, leading to variations in gene expression, cell function, morphology, and extracellular matrix (ECM) remodeling. As the mechanisms involved during bone remodeling are the same as those found during fracture healing [McKibbin, 1978], it is thus reasonable to consider mechanical stimulations as a therapeutic strategy to induce healing in a bone fracture. Recently, the use of superparamagnetic scaffolds to provide mechanical stimulation by external EMF has attracted great interest [Zeng et al., 2012; Meng et al., 2013; Xu and Gu, 2014; Grant et al., 2015]. The presence of superparamagnetic nanoparticles (NPs) alter the mechanical properties of organic scaffolds by manipulating the compressive strength and elastic modulus. Superparamagnetic NPs become magnetized when exposed to magnetic fields, when these fields are alternating, such as EMFs, inducing their vibrational and rotational displacement. When these NPs are within a scaffold, these vibrational and rotational forces induce mechanical changes in the scaffold and anything attached to it, such as the cells [Corona-Gomez et al., 2016; Hasan et al., 2018]. The improved mechanical properties in three-dimensional (3D) scaffolds, particularly elastic modulus values, have been shown to promote MSC osteogenic differentiation [Jegal et al., 2011]. Polymer-based nanocomposite scaffolds loaded with magnetic particles are used in drug delivery applications [Edelman et al., 1984; Liu et al., 2006; Zhao et al., 2011]. Recently, the use of Fe_3O_4 superparamagnetic scaffolds and standard EMFs has been proposed to promote the bone formation [Kanczler et al., 2010; Sapir-Lekhovitser et al., 2016]. This approach capitalizes on coupling of two separate stimuli on the cells: mechanical, through the vibratory movement of the scaffold where the cells are attached and magnetic, where the EMF can change the transmembrane potential through the regulation of various ion channels and transporters [Deng et al., 2007; Garner et al., 2007]. There is mounting evidence supporting the functional role of the transmembrane potential in regulating the proliferation and differentiation of MSCs [Sundelacruz et al., 2008; Sundelacruz et al., 2009; Hronik-Tupaj et al., 2011].

In this study, we used a biomimetic scaffold based on the self-assembling peptide RADA16, consisting of regular repeats of alternating ionic hydrophilic and hydrophobic amino acids. The interwoven nanofibers of RAD16 forms higher order hydrogels with unique biomechanical properties that could be comparable with the natural ECM, making them good candidates to generate biomimetic cell niches [Semino, 2008]. Furthermore, these multifunctional superparamagnetic scaffolds are synthesized by either the addition of Fe_3O_4 superparamagnetic NPs to the pre-formed scaffolds by dip-coating in NP solutions or by mixing the two during scaffold synthesis. We report on the cell proliferation and differentiation of human adipose-derived mesenchymal stem cells (hASCs) grown on self-assembled peptide hydrogels containing superparamagnetic iron oxide NPs after being biochemically stimulated with osteogenic induction media and/or extremely low-frequency pEMFs.

MATERIALS AND METHODS

Cell Culture

The hASCs purchased from Lonza (Walkersville, MD) were cultured under standard culture conditions in a sterile, humidified incubator at 37°C, and 5% CO_2/95% air. The cells were cultured in T75 flasks at a density of 5.0×10^5 cells/flask, using MSC growth medium (Msc media) purchased from ScienCell (Carlsbad, CA) that consisted of 500 ml basal medium, 5 ml MSC growth supplement (MSCGS), and 5 ml of a penicillin/streptomycin solution. The appropriate amount of MSC media was added to each flask (0.2–0.4 ml/cm^2) and was replaced every 3 days. The cells used in all experiments were from the fourth passage.

3D Cell Encapsulation and Gel Formation

To prepare the 3D cell culture, self-assembled peptides PuraMatrix composed of standard amino acids (1% w/v) and 99% water were purchased from Corning (New York, NY). The encapsulation of cells within the hydrogel scaffold followed the manufacturer's instructions. In brief, PuraMatrix stock solution (1% w/v) was sonicated for 30 min in the ultrasonic bath to remove air bubbles and reduce its viscosity.

Then, the required amount of PuraMatrix stock was aliquoted and mixed with 20% sterile sucrose at a 1:1 ratio to yield a 0.5% w/v concentration (half of the 20% sucrose was mixed with the gel and the other half with suspended cells). At this point, formulations including 10 nm carboxy-functionalized superparamagnetic iron oxide NPs (Sigma-Aldrich, St. Louis, MO) were added at a concentration of 0.5% of the total volume of the mixed solution. Subsequently, the cell suspension was prepared trypsinizing the flasks with a 0.25% trypsin/EDTA solution purchased from ScienCell (Carlsbad, CA). The cells (1.5×10^5 cells/well) were resuspended in sterile 20% sucrose. The cells/sucrose mixture was mixed equally with hydrogel mixture, to be transferred quickly to the center of 24-well plates with total volume of 150 µl/well, and 750 µl media was added to form the gel in each well. As the PuraMatrix pH is 2–2.5, the media was changed twice to allow it to equilibrate to the physiological pH of the 3D cell culture.

Cell Viability

Lactate dehydrogenase (LDH) assay (CytoTox 96R Assay kit) purchased from Promega (Madison, WI) was used to evaluate the cytotoxicity and proliferation of cells cultured within the hydrogel. LDH is a stable cytosolic enzyme that can be measured from the cell lysate, which reacts with a tetrazolium salt (i.e. iodonitrotetrazolium violet) to form a deep red formazan dye. The number of cells was assessed during specific intervals (i.e. 7, 14, and 21 days) according to the manufacturer's protocol. In brief, to prepare the lysis samples, the cells-gel constructs were treated with collagenase to digest the collagen secreted from the cells. The samples were incubated in 50 µl of collagenase for 30 min after washing with phosphate-buffered saline (PBS). Later, each sample was mixed with 500 µl of lysis buffer (1% Triton X-100), then sonicated for 1 h. The samples were then centrifuged at high speed. Next, 50 µl of the supernatant and 50 µl of CytoTox 96 reagent were added to each well of a 96-well plate and covered with foil for 30 min at room temperature. Then, 50 µl of the stop solution was added to each well. Absorbance at 492 nm was recorded and using the calibration curve, the cell number was quantified.

Differentiation Assay

The alkaline phosphatase (ALP) assay was used to detect the osteogenic differentiation of hASCs. ALP is an early osteogenic marker expressed on the cell surface. SensoLyte pNPP Alkaline Phosphatase Assay Kit (AnaSpec, Fremont, CA) was used by measuring the absorbance at 405 nm. In brief, after removing the growth medium from each sample and washing with PBS, 50 µl of collagenase was added and incubated for 30 min. Then, 500 µl lysis buffer (1% Triton X-100) was added to each well. The cell lysate was ready after sonication for 1 h and centrifuging at 10,000 rpm for 5 min. Then, 50 µl of lysate cells was added to 96-well plate with a flat bottom, and 50 µl of pNPP substrate solution was added to detect the ALP. Upon dephosphorylation of pNPP, the lysate samples turned yellow. After incubation for 30 min at 37°C, 50 µl of stop solution was added to stop the reaction. With the absorbance reading from the microplate reader, the ALP secretion was quantified using the calibration curve. Then, the data were normalized with the total number of cells per well, expressing the ALP concentration in ng/cell. This assay was performed at 7, 14, and 21 days of incubation in triplicate.

Mineralization

Mineralization on the constructs was quantified by using Inductively Coupled Plasma-Optical Emission Spectroscopy (ICP-OES, 710-ES; Varian, Palo Alto, CA) detecting calcium at 7, 14, and 21 days of incubation ($n = 3$). The samples were decalcified in 35% HCl (trace metal grade; Fisher Chemical, Pittsburgh, PA), followed by boiling for 5 h at 90 °C. Then, the samples were collected in liquid form, and calcium was measured with ICP-OES through emissions at 396 nm. From the emission intensity, the calcium concentration is obtained in mg/L (ppm) using a calibration curve.

Cell Morphology

To investigate cell morphology in response to variations in the extracellular environment, cytoskeletal actin microfilaments (F-actin) were stained using fluorescent phalloidin conjugates (F-actin visualization Biochem kit; Cytoskeleton, Denver, CO). Also, 4′, 6-diamidino-2-phenylindole, dihydrochloride (DAPI) was used to stain the cell's nucleus. This experiment was performed at days 3 and 14, and the results were visualized using confocal microscopy (FV1000; Olympus, Center Valley, PA) with an excitation/emission filter for F-actin (535/585 nm) and DAPI (358/461 nm). The staining was done according to the manufacturer's instructions. In brief, after removing the media from each sample and washing with washing buffer, 200 µl of the fixative solution was added for 10 min. Then, the samples were washed twice with washing buffer to remove the fixative materials, and 200 µl of permeabilization buffer was added to each fixative sample. After 5 min, each

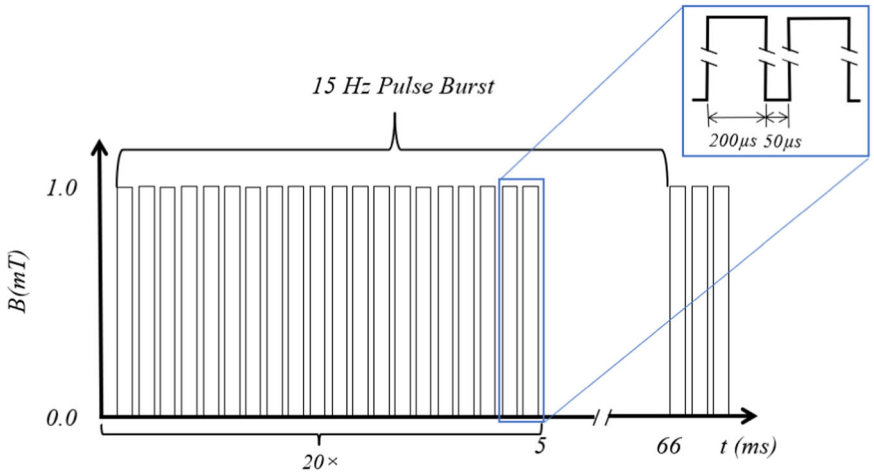

Fig. 1. Pulsed electromagnetic field (EMF) burst waveform. The pulsed 1 mT signal repeated 20 times with a pulse frequency of 15 Hz, which lies in the extremely low-frequency range. Individual 250 μs pulses constitute a 4 kHz repetition frequency. Inst: Details of the individual pulses showing an 80% duty cycle.

sample was washed twice with washing buffer. A 0.165 μM F-stain phalloidin and 300 nM DAPI solution was prepared, then the stained sample was covered with foil to keep it dark for 30 min at room temperature. Then, each sample was washed three times to stop the reaction and covered with mounting medium and coverslip.

ALP Staining

For qualitative investigation of cell differentiation, ALP Staining Kit II (Stemgent, Cambridge, MA) was used to detect ALP activity within the samples at day 14. In brief, after removing the media, the samples were washed with 0.05% concentration of PBS containing Tween-20 as permeabilizing agent, and 0.5 ml of fixative solution was added for 5–10 min. Then, the samples were washed twice, and 0.6 ml of ALP staining was added, which was composed of equal ratio 1:1:1 of ALP substrate solution (a mixture of 0.2 ml of solution A and 0.2 ml of solution C), for 15 min at room temperature. For stopping the reaction, the samples were washed twice with PBS. Later, the samples were covered with mounting medium and coverslip to prevent drying. Through use, the ALP expression was detected as a red or purple stain.

pEMF Stimulation

The goal of this study was to expose hASCs to a pEMF equivalent to the one published by Bassett et al. [1982], as it was the basis for Class III EMF devices approved by the FDA within the category of bone growth simulation stimulation [Daish et al., 2018]. For that we used Helmholtz coils capable of generating a 1 mT field. We added superparamagnetic NPs to see if we could enhance the osteogenic differentiation, expecting this to be mainly a mechanically stimulatory effect. The extremely low-frequency-generating pEMF equipment consisted of a function generator, oscilloscope, Helmholtz coils, and μ-metal box. The function generator (33220 A; Agilent Technologies, Santa Clara, CA) generated the burst signal with specific frequency, amplitude, and shape (Fig. 1). The test signal was equivalent to FDA approved signal for bone fracture healing, which consisted of 15 Hz pulse burst of 20 pulses with magnetic field intensity of 1 mT for a total 5 ms and then decreasing to zero in 61 ms [Bassett et al., 1982; Daish et al., 2018; Polo-Corrales et al., 2018]. Each pulse increased from 0 to 1 mT and remained at that level for 200 μs, resting for 50 μs and repeating for 19 additional identical pulses. An oscilloscope (model MSO 6012A; Agilent Technologies) was used to display the generated signals in terms of voltage as a function of time. The EMF was generated using Helmholtz coils (3B U8481500; 3B Scientific, Tucker, GA), which consisted of a pair of copper coils that operate on alternating fields. When an alternating current ran through the Helmholtz coils, uniform EMFs were generated in space over a considerable volume. The samples were placed in the center of the coils where each coil consisted of 124 turns, outer coil diameter was 311 mm, inner coil diameter was 287 mm, mean coil radius was 150 mm, and coil resistance was 1.2 Ω. The magnitude of magnetic flux density (B) is calculated according to the following formula [Gupta et al., 1991]:

$$B = \left(\frac{5}{4}\right)^{\frac{3}{2}} \mu_0 I \frac{n}{R} \quad (1)$$

where n is the number of turns in each coil, I is the current, R is the mean coil radius, and μ_0 is the permeability of free space ($4\pi \times 10^{-7}$ T·m/A), which leads to $B = 7.433 \times 10^{-4}\, I$ in T.

The Helmholtz coils were placed in the incubator inside a μ–metal enclosure (a box custom-made in-house using MuMETAL; Magnetic Shield Corporation, Bensenville, IL) which was shielded against the external fields, such as earth static fields and low magnetic fields from the surrounding equipment. This ensured that the only EMF exposure came from the Helmholtz coils. The μ–metal was composed of nickel, iron, and some copper or chromium that gave a low reluctance path for the magnetic flux. A commercially available thermocouple (RSC-12; Omega, Stamford, CN) was used to monitor the temperature in the proximity of the microwell plates. The pEMF system maintained a temperature of 37 ± 0.7 °C during 8 h of operation, chosen based on its frequency of use in the published results [Schwartz et al., 2008; Zhao et al., 2008; Sun et al., 2009, 2010; Zhong et al., 2012; Ceccarelli et al., 2013; Kang et al., 2013]. The experimental groups were divided into two: pEMF-stimulated and non-stimulated. Each experimental group consisted of four different formulations, all based on hASC-seeded scaffolds, with/without Osteo media (osteogenic induction media consist of mesenchymal stem cell osteogenic differentiation medium from ScienCell), and with/without NPs. The stimulated group was exposed to pEMFs for 8 h every day. The non-stimulated group was placed in the pEMF system for 8 h per day but it was kept off.

Statistical Analysis

We tested four different formulations, all based on passage 4 hASC-seeded scaffolds, with/without osteogenic induction media, with/without NPs, and with/without pEMF stimulation. Each of the four formulations consisted of three technical replicate wells, whose values were averaged to form each independent data point. In addition, for each experimental condition (i.e. with/without pEMF) the experiments were run in triplicate (i.e. biological replicates). All numerical data were evaluated statistically according to the analysis of variance (ANOVA) test followed by Dunnett test to identify the significant differences. Values of $P < 0.05$ were accepted to be used as a significant level of difference between the mean of the experimental and corresponding control groups. The mean values were calculated from the average results of three independent samples; the results are represented as mean $\pm$ standard deviation (SD).

RESULTS

Viability and Proliferation

The cell proliferation was quantified using an LDH cytotoxicity assay using passage 4 hASCs for four different formulations that were either pEMF-stimulated or non-stimulated. The results were assessed after 7, 14, and 21 days of culture for all formulations. The results showed that the cells start to grow rapidly for all groups (Fig. 2). However, no statistically significant difference was seen in cellular viability between groups with and without pEMF stimulation.

At day 7, within the non-stimulated (i.e. osteogenic induction media) group there was a significant increase ($P < 0.001$) in the number of viable cells detected within the superparamagnetic (NP-containing) scaffold over those using the hydrogel alone. This suggested that the carboxy-functionalized iron oxide NPs promote cell proliferation. It is known that carboxy functionalities increase hydrophilicity and significantly increase the proliferation and osteogenic differentiation of MSCs [Phillips et al., 2010]. It has also been shown that by using electrospun superparamagnetic scaffolds based on γ-Fe_2O_3/nano-hydroxyapatite/poly-lactic acid, the proliferation of pre-osteoblasts can be enhanced, compared with scaffolds lacking the superparamagnetic NPs [Meng et al., 2010]. However, the group of superparamagnetic scaffolds under pEMF stimulation (i.e. without osteogenic induction media) showed similar proliferation rates to the non-stimulated group, which were significantly different ($P < 0.001$) to the control (i.e. lacking NPs). The biochemical stimulation using osteogenic induction media alone was enough to significantly ($P < 0.001$) enhance cell proliferation when compared with the non-stimulated control. Although this significant increase in the rate of proliferation was also seen in both pEMF-stimulated and non-stimulated superparamagnetic scaffold groups, there was no significant difference between them, but only with respect to the control ($P < 0.0001$).

At day 14, all the groups continue to grow, under basal media, with similar proliferation rates, with no significant differences between pEMF-stimulated and non-stimulated groups, regardless of the presence of NP-containing superparamagnetic scaffolds, when compared with the control. When the cells were stimulated with osteogenic induction media, no significant differences between pEMF-stimulated and non-stimulated groups was observed in the hydrogel alone, while a significant difference was seen in the control ($P < 0.05$).

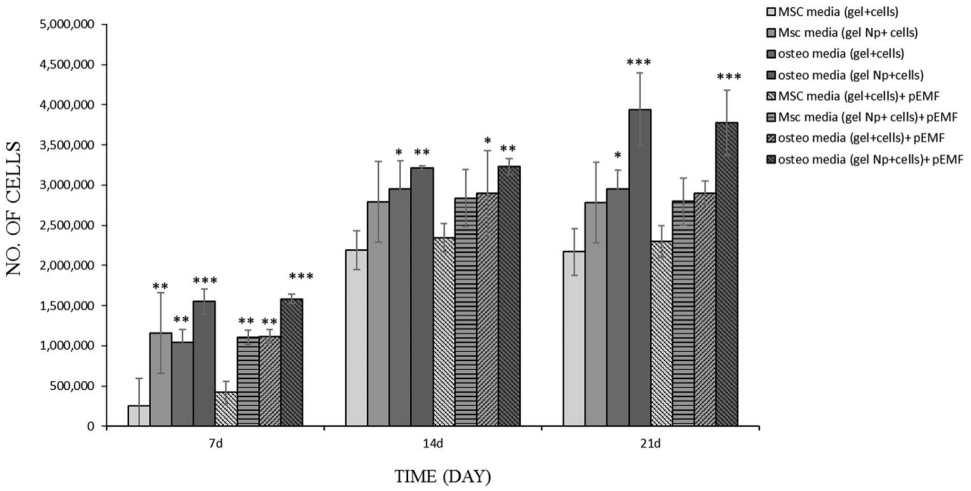

Fig. 2. Lactate dehydrogenase (LDH) assay. The proliferation of human adipose-derived mesenchymal stem cells (hASCs) seeded within self-assembled peptide hydrogel with and without nanoparticles (NPs) under extremely low-frequency pulsed electromagnetic field (pEMF) of 1 mT were quantified, after 7, 14, and 21 days. $^{*}P < 0.05$; $^{**}P < 0.001$; and $^{***}P < 0.0001$, indicate statistically significant differences between basal media group (control) and the other groups. The mean values are calculated from the average results of three samples; the results are represented as mean ± standard deviation (SD).

On the contrary, there was a significant difference ($P < 0.001$) when the cells were grown in superparamagnetic scaffolds, showing enhanced cellular proliferation when pEMF-stimulated. At day 21, the same trend was observed as seen at day 14. In addition, the group stimulated with osteogenic induction media was significantly different ($P < 0.05$) from the control.

Differentiation

Osteoblast differentiation from hASCs was detected measuring the activity of the ALP biomarker after 7, 14, and 21 days of culture [Wang et al., 2007]. As before, the two experimental groups were tested, pEMF-stimulated and non-stimulated, which were subdivided into four different formulations, all based on hASC-seeded scaffolds, with/without osteogenic induction media, and with/without NPs. ALP activity at day 7 showed signs of early differentiation of hASCs cells into osteoblasts (Fig. 3). However, the cells cultured within the group of superparamagnetic scaffolds under pEMF stimulation (i.e. without osteogenic induction media) showed a low level of ALP activity, statistically similar to the non-stimulated group and controls (i.e. with and without pEMF stimulation, and both lacking NPs). However, when the hASCs in hydrogels (no NPs) were simultaneously stimulated with osteogenic induction media and pEMF, they demonstrated signs of an early osteoblast differentiation with a significant increase in ALP activity ($P < 0.05$), when compared with the control. In contrast, a lack of pEMF stimulation showed low levels of ALP activity with no significant difference in the control. Under these conditions, the presence of superparamagnetic scaffolds shows high levels of ALP activity with a significant difference ($P < 0.001$) without pEMF stimulation and even higher with pEMF stimulation significantly higher than the control ($P < 0.0001$). Although, after 14 days of culture, the levels of ALP activity had significantly increased in all groups, those using superparamagnetic scaffolds (i.e. without osteogenic induction media) with and without pEMF stimulation showed no significant difference when compared with the control. In the case of the group under pEMF stimulation (without NPs or osteogenic induction media), it showed a slight increase of ALP activity, although not significant when compared with the control.

However, when the cells were stimulated with osteogenic induction media (i.e. without pEMF) there was a significant increase in differentiation, as measured by ALP activity ($P < 0.001$), with the addition of pEMF stimulation, showing a significant increase ($P < 0.05$). The results at day 7 revealed that the presence of superparamagnetic scaffolds led to elevated levels of ALP activity significantly different ($P < 0.001$) to those without pEMF stimulation and even significantly higher to those with pEMF stimulation ($P < 0.0001$). At day 21, an increase in the ALP activity with time could still be seen, with the groups with osteogenic induction, regardless of the presence of pEMF stimulation, being significantly different from the control ($P < 0.0001$). Similarly, the

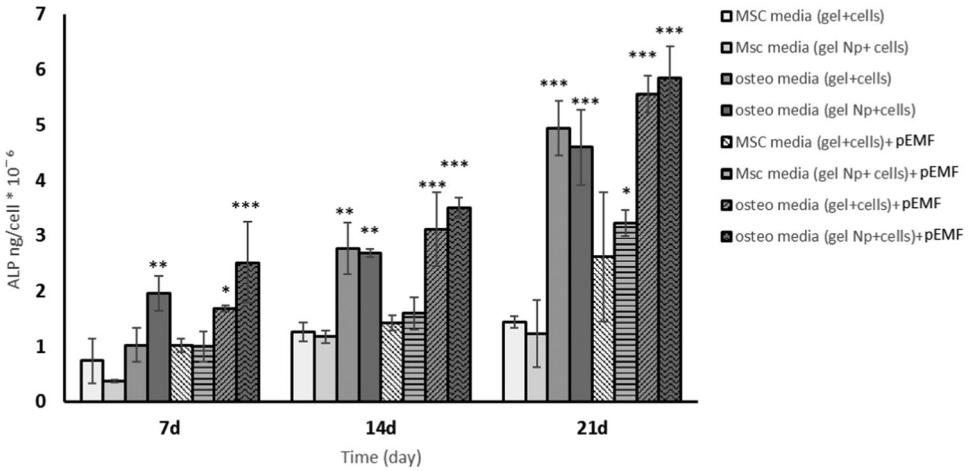

Fig. 3. Alkaline phosphatase (ALP) activity. The differentiation of human adipose-derived mesenchymal stem cells (hASCs) was assessed at 7, 14, and 21 days. ALP values were normalized with the number of cells of each sample. $^{*}P < 0.05$; $^{**}P < 0.001$; $^{***}P < 0.0001$ indicate statistically significant differences between basal media group (control) and the other groups (one-way analysis of variance [ANOVA] followed by Dunnett's test). The mean values are calculated from the average results of three samples; the results are represented as mean ± standard deviation (SD).

presence of superparamagnetic scaffolds was significantly different from the control ($P < 0.0001$). Moreover, ALP activity had significantly increased ($P < 0.05$) for the first time for the superparamagnetic scaffold group without osteogenic induction media, but with pEMF stimulation, while the other groups remain unchanged.

Mineralization

While ALP is a relatively early differentiation marker that increases during the proliferation and matrix synthesis stage [Harris, 1990], the matrix calcium deposition defines the terminal stage in osteoblast maturation [Cormier, 1995]. Therefore, the series of osteogenic differentiation assays involving ALP activity and staining, and the calcium mineralization, demonstrates the significant role the 3D superparamagnetic scaffolds played in accelerating osteoblastogenesis of hASCs. The calcium depositions were quantified for all the groups over three weeks (i.e. at days 7, 14, and 21) as shown in Figure 4.

We were not able to detect any calcium depositions for four of the experimental groups at day 7. These included the hASC-seeded scaffolds, with pEMF stimulation, with osteogenic induction media stimulation, and NP-containing superparamagnetic scaffolds without any stimulation. However, the group with NP-containing superparamagnetic scaffolds stimulated with induction media showed some early calcium deposition. Also, although the remaining three groups, which were all pEMF-stimulated, showed some early calcium deposition, it was not significantly different from the superparamagnetic scaffold stimulated with only osteogenic induction media. These groups were superparamagnetic scaffolds with and without induction media and hydrogel scaffolds (without NPs) with induction media, all three being pEMF-stimulated. After 7 days, non-significant trace of calcium in the ECM was observed. This was true for groups with pEMF stimulation or osteoinductive media without pEMF. After 14 days, even the hASC-seeded control (i.e. without stimulation) started to show traces of calcium in the ECM. Meanwhile, the groups with superparamagnetic scaffolds stimulated with induction media, and with and without pEMF stimulation, showed higher levels of calcium deposition, but not significantly higher than the control. After 21 days, there was a significant increase ($P < 0.05$) in calcium deposition, in all groups being pEMF-stimulated, when compared with those that were not.

Cell Morphology

A qualitative test was used to image cells using actin and DAPI staining, as shown in Figure 5, for days 3 and 14. At day 3, after culturing the cells within the hydrogel alone, with and without pEMF stimulation (without induction media), many of the cells could be seen with a spherical shape as they settled into the 3D hydrogel (Fig. 5A, B, E, and F, day 3). In contrast, the groups stimulated with osteogenic induction media showed a spindle and elongated morphology in the case of both pEMF-stimulated and

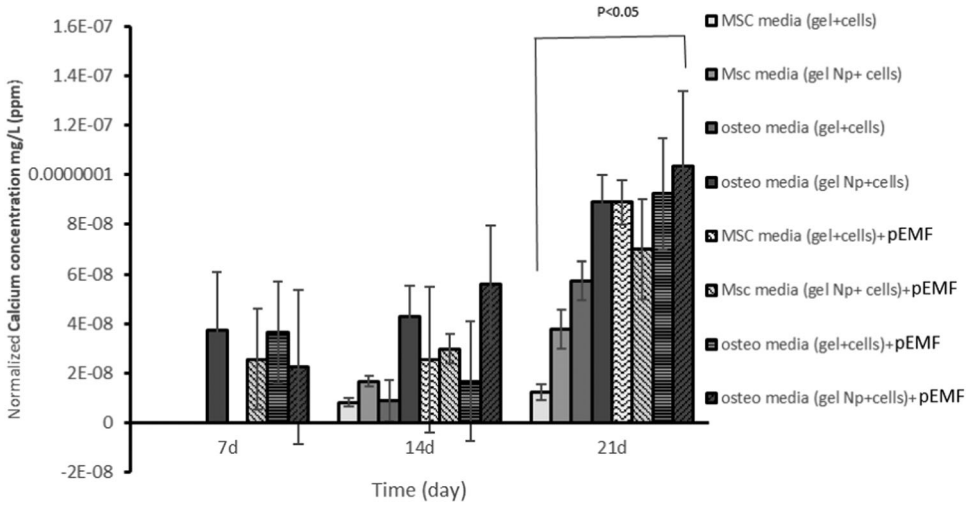

Fig. 4. Mineralization assay. Calcium concentrations were quantified after 7, 14, and 21 days. Error bar represents the standard deviation (SD). $P < 0.05$ indicates statistically significant differences between mesenchymal stem cells (MSCs) media gel + cells group (control) and the other groups (one-way analysis of variance [ANOVA] followed by Dunnett's test). The mean values are calculated from the average results of three samples; the results are represented as mean ± SD.

non-stimulated groups, showing early signs of osteoblastic differentiation (Fig. 5C, D, G, and H, day 3). Others showed the same behavior, where the elongated cells represented signs of differentiation or specialization into osteoblasts, following adherence to the scaffold. At day 14, the images showed that the cells were entirely embedded in the hydrogel, taking the shape of its fibers (Fig. 5, day 14).

ALP staining

To do a qualitative evaluation of hASCs osteoblast differentiation, ALP staining was used at day 14 for all eight groups as shown in Figure 6. The results demonstrate that at day 14, hASCs had differentiated into osteoblasts. Whereas the groups that were cultured with and without NPs, and without pEMF or induction media showed only marginal ALP staining (Fig. 6A and B), when they were pEMF-stimulated, they showed high levels of ALP staining (Fig. 6E and F). In addition, the results showed higher levels of ALP staining when stimulated with osteogenic induction media, with or without pEMF stimulation (Fig. 6C, D, G, and H).

DISCUSSION

In this study, the results from the proliferation assay showed no cytotoxicity from the hydrogel with or without the presence of NPs toward hASCs, showing an appreciable proliferation rate. The assessment of biochemical (i.e. osteogenic induction media), mechanical, and electromagnetic stimulation on hASC proliferation showed that the simultaneous presence of osteogenic induction media and superparamagnetic NPs had the strongest effect on cell proliferation, without any significant impact by pEMFs. This lack of effect due to pEMF stimulation on proliferation was also seen in the non-stimulated (i.e. biochemical and mechanical) controls. The presence of either osteogenic induction media or superparamagnetic NPs had an equivalent positive effect on hASC proliferation, though this positive effect was significantly less than the combined presence of osteogenic induction media and NPs.

The objective of adding superparamagnetic NPs to the hydrogel was to induce a mechanical vibration on its matrix with the application of an alternating magnetic field [Golovin et al., 2017]. The results suggested that although the presence of superparamagnetic NPs promotes hASC proliferation, the mechanical vibration that should have been induced by the pEMFs is not required or present. It must thus be an intrinsic property of the NPs, which is the cause of the increase in cell proliferation, and that further boosts this effect in the presence of osteogenic induction media. This is consistent with the published results showing the osteoinductive effects of superparamagnetic NPs without the application of external magnetic fields [Wu et al., 2010; Wei et al., 2011; Yun et al., 2015]. Although many of the studies reporting this effect do not provide possible mechanisms to explain this phenomenon, some have explored different hypotheses [Castro et al., 2017; Zhu et al., 2017]. A very thorough

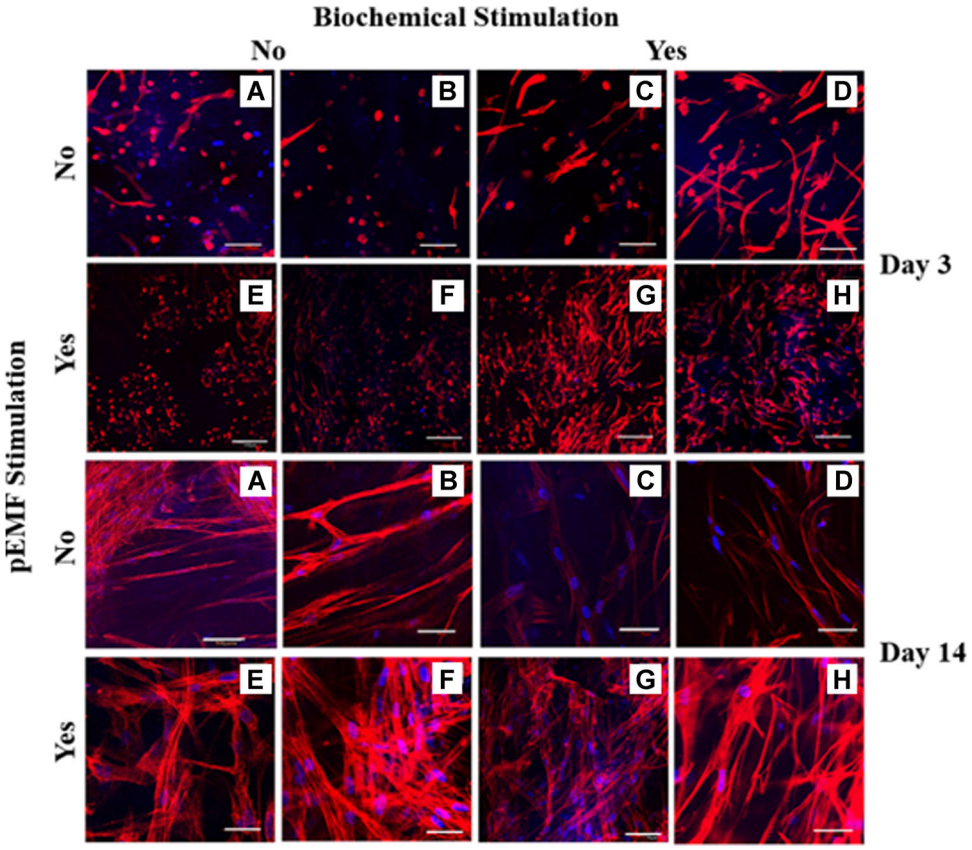

Fig. 5. Phalloidin-labeled actin filaments stain (red) and 4′,6-diamidino-2-phenylindole (DAPI), dihydrochloride stain (blue) for human adipose-derived mesenchymal stem cells (hASCs) within hydrogel at days 3 and 14. (**A**) Basal media, (**B**) basal media + nanoparticles (NPs), (**C**) osteogenic media, (**D**) osteogenic media + NPs, (**E**) basal media + pulsed electromagnetic field (pEMF), (**F**) basal media + NPs + pEMF, (**G**) osteogenic media + pEMF, (**H**) osteogenic media + NPs + pEMF. Scale bars at days 3 and 14 are 100 μm (×10) and 51 μm (×20), respectively. Biochemical stimulation—osteogenic induction media.

and interesting study proposed that the composition of the protein corona that forms on the superparamagnetic NPs could provide the necessary stimulation to promote the measured levels of proliferation. The study characterized the protein composition of the corona after being exposed to fetal bovine serum alone or in the presence of proteins secreted by pre-osteoblasts [Zhu et al., 2017]. Their findings showed the presence of proteins related to calcium ions, G-protein coupled receptors, and MAPK/ERK cascades as compared with scaffolds not containing NPs. All these could be related to help in the induction of cell proliferation and could thus explain the increase in hASC proliferation in the presence of superparamagnetic scaffolds without pEMF stimulation.

The other question posed by these results is if a magnetic field of 1 mT, like the one used in this study, was enough to generate enough force on the NPs to mechanically stimulate the cells. It has been shown that the estimated force needed for the stimulation of single mechanosensitive channel is as low as 1–2 pN [Yoshimura and Sokabe, 2010], while another study demonstrated that the estimated mechanical force of 0.2 pN was required to activate the TREK-1 channel and 2 pN to break the bond between fibronectin and the cytoskeleton [Sapir-Lekhovitser et al., 2016]. To estimate the magnetic force generated on each cell to activate the mechanotransduction process, we decided to calculate the total force and divide it by number of cells in each well plate. Our results showed (see Supplementary Information) that the calculated magnetic force was about 0.148 pN per cell and its influence was noticed for the group of cells with NPs in the presence of pEMF stimulation during the first week of culture as compared with the control ($P < 0.001$). Nevertheless, after 14 and 21 days the magnetic force per cell was not strong enough to

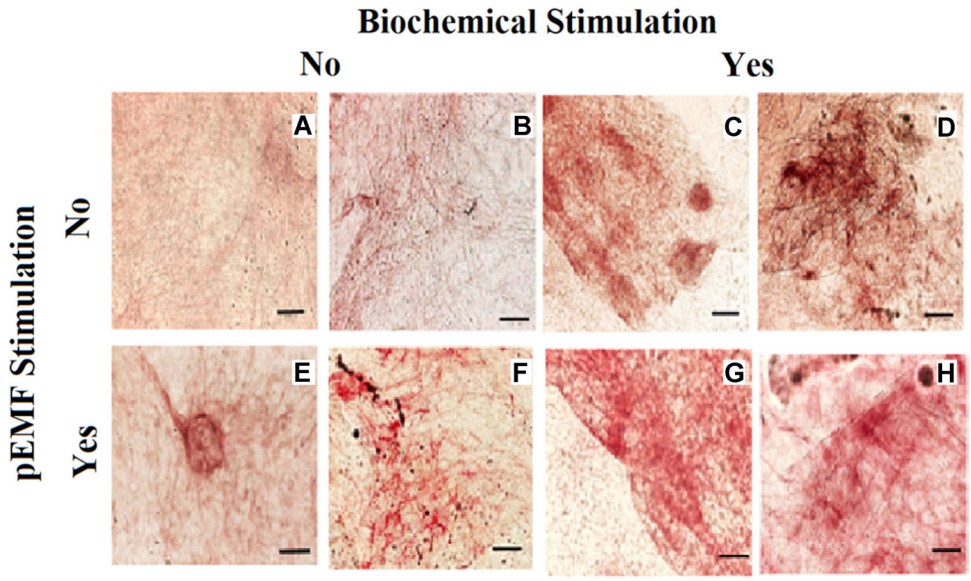

Fig. 6. Alkaline phosphatase stain for human adipose-derived mesenchymal stem cells (hASCs) seeded within hydrogel at day 14, scale bar = 200 μm (×10). (**A**) Basal media, (**B**) basal media + nanoparticles (NPs), (**C**) osteogenic media, (**D**) osteogenic media + NPs, (**E**) basal media + pulsed electromagnetic field (pEMF), (**F**) basal media + NPs + pEMF, (**G**) osteogenic media + pEMF, (**H**) osteogenic media + NPs + pEMF. Biochemical stimulation—osteogenic induction media.

activate the mechanotransduction pathway, simply because cells had proliferated while the number of NPs remained the same, lowering the capacity of the superparamagnetic scaffold to stimulate the cells. Both groups of cells under pEMF with and without NPs showed significant changes as compared with the control, but this effect was not necessarily from NPs.

The results from the ALP assay showed that the hASCs start to differentiate into the osteoblast phenotype from day 7, when grown in the superparamagnetic scaffold and cultured with osteogenic induction media. Also, early differentiation at day 7 was noticed in the group cultured within osteogenic media, with and without pEMF stimulation, with ALP activity being higher in the latter. These effects were not seen in the presence of osteogenic induction media alone, but only after 14 days of stimulation. At this same time, it can also be seen that hASCs biochemically stimulated with induction media and continued to increase their level of differentiation, with a non-significant increase in presence of pEMF stimulation and a non-significant difference due to the presence of NPs. After 2 weeks a trend starts to emerge, which involved a significant level of osteogenic differentiation by hASCs stimulated with osteogenic induction media, with a non-significant increase due to pEMF stimulation and no effect due to the superparamagnetic scaffolds. If the proposed NP protein corona mechanism [Zhu et al., 2017] is correct, then the significant difference in ALP activity seen after 7 days in the presence of superparamagnetic scaffolds is due to osteogenic media proteins adsorbed onto the NPs and inducing hASC differentiation. During this initial stage, there is a sustained presence of osteogenic media proteins, which allows an early commitment of hASC to the osteogenic lineage [Robert et al., 2018]. After lineage commitment, there is less need of osteogenic proteins to continue the differentiation process [Ferroni et al., 2018]. So, the presence of the superparamagnetic scaffolds helps improve the levels of hASC osteogenic differentiation by allowing an early commitment of these cells to the osteogenic lineage.

Groups with low initial (i.e. days 7 and 14) ALP activity did not form much mineralized matrix after 21 days, especially the control group. However, mineralization measurements support the ALP activity results, whereas the samples that were cultured in superparamagnetic scaffolds and osteogenic induction media showed an early calcium deposition, and increased the ALP activity, after 7 days. In fact, this effect can be present during the first 2 weeks. As expected, the ALP staining results were consistent with the quantitative ALP activity results. At day 14, the biochemically stimulated cells showed high levels of alkaline phosphatase, with a non-significant increase due to the presence of pEMF stimulation and a non-significant difference in the presence of NPs.

There is a clear and significant increase in mineralization after 21 days, due to pEMF stimulation. As the results show, the hASCs had already differentiated and did not need further stimulation from the induction media or NPs and are depositing mineral stimulated solely by pEMFs. The group with osteogenic media and NPs had high ALP activity from the very first week of culture (day 7) and showed no significant mineralization compared to the control. We believe that the cells in this group differentiated very early and started immobilizing calcium earlier than groups exposed to pEMF stimulation, so the ECM calcium was comparable with the group with pEMF stimulation at day 21.

The results on hASC morphology showed that the cells interacted intimately with the ECM as the scaffold was mainly composed of water, allowing the cells to freely migrate and interact. Also, the presence of NPs or EMFs did not affect cell morphology. During the early days of seeding, the hASCs adopted a spherical shape, but later they started to elongate and got spindle morphology. Fan and Wang [2017] mentioned that the hASCs need to adhere to a surface to allow them to stretch and be able to make contact with other cells; if not they will become apoptotic.

In this study, we developed a superparamagnetic scaffold based on a biomimetic hydrogel for the 3D culture of hASCs to study their response to biochemical, electromagnetic, and putative mechanical stimulation. This was done by evaluating proliferation, osteoblastic differentiation, ECM mineralization, and morphology under a combination of these forms of stimulation. The 3D superparamagnetic scaffold was based on peptides that self-assembled to form nanofibers and an ECM-type of structure that allows nutrients and oxygen to be effectively transported to the seeded cells in a manner similar to the natural condition [Zhang, 2004]. Hydrogels made from these peptides have demonstrated the capacity to enhance the proliferation and differentiation of primary osteoblasts in vitro [Bokhari et al., 2005] and in vivo [Misawa et al., 2006]. The choice of hASCs over bone marrow-derived MSCs was based on their capacity to proliferate faster and retain an enhanced capacity for differentiation over their bone marrow counterparts [Burrow et al., 2017].

CONCLUSIONS

Our results show no negative or cytotoxic effects on hASCs due to the presence of pEMFs or superparamagnetic NPs. Also, the results showed that there was an early differentiation by incorporating osteogenic media in the presence of either superparamagnetic NPs or pEMFs that could not be achieved by osteogenic media alone. The principal results of the present study revealed several novel findings regarding the events involved in the induction of the osteogenic differentiation of hASCs by pEMFs and putative mechanical stimulation; for instance, that addition of superparamagnetic NPs to the hydrogel induced a significant increase in proliferation. This could be the result of either NP vibration or their protein corona, or a combined effect. On the basis of the force per cell calculated at day 7 (see Supplementary Material), we suggest that there was a vibratory force strong enough to stimulate each cell in the presence of pEMFs, in addition of that from the protein corona on the NPs in the presence of pEMFs, allowing the highest proliferation rate seen for that time point. In contrast, at days 14 and 21, the higher proliferation rates were not likely due to NP vibrations (i.e. putative mechanical stimulation) as there was a higher number of cells while the number of NPs remained the same. We propose that the proliferative effect at days 14 and 21 was solely due to the proteins adsorbed onto the NPs. Perhaps increasing the intensity of the magnetic field and/or the amount of NPs in the scaffold will actuate a level of vibration in the superparamagnetic NPs to mechanically stimulate the hASCs until a mature tissue construct is formed [Golovin et al., 2017]. In addition, it was seen that after two weeks there were significant levels of osteogenic differentiation of hASCs stimulated with osteogenic induction media, with no increase under pEMF stimulation and no effect due to the superparamagnetic scaffolds. Perhaps prior to that, due to the sustained presence of osteogenic media proteins on the corona of the NPs, there was an early commitment of hASC to the osteogenic lineage. Committed cells then became significantly more responsive to pEMF stimulation, not only promoting osteogenic differentiation, as evidenced by ALP activity and staining, or the extent of ECM mineralization [Ferroni et al., 2018]. It is important to mention that although in this study we used what we considered to be a standard set of parameters (i.e. frequency, intensity, and time of exposure), a thorough study assessing parameter sensitivity to hASC differentiation capacity is needed to allow proper replication and optimization of the pEMF effects [Ross et al., 2015].

REFERENCES

Ayala MR, Syrovets T, Hafner S, Zablotskii V, Dejneka A, Simmet T. 2018. Spatiotemporal magnetic fields enhance cytosolic Ca^{2+} levels and induce actin polymerization via activation of voltage-gated sodium channels in skeletal muscle cells. Biomaterials 163:174–184.

Bassett CAL, Mitchell SN, Gaston SR. 1982. Pulsing electromagnetic field treatment in ununited fractures and failed arthrodeses. JAMA 247:623–628.

Bokhari MA, Akay G, Zhang S, Birch MA. 2005. The enhancement of osteoblast growth and differentiation in vitro on a peptide hydrogel—PolyHIPE polymer hybrid material. Biomaterials 26:5198–5208.

Burrow KL, Hoyland JA, Richardson SM. 2017. Human adipose-derived stem cells exhibit enhanced proliferative capacity and retain multipotency longer than donor-matched bone marrow mesenchymal stem cells during expansion in vitro. Stem Cells Int 2017:2541275.

Castro PS, Bertotti M, Naves AF, Catalani LH, Cornejo DR, Bloisi GD, Petri DF. 2017. Hybrid magnetic scaffolds: The role of scaffolds charge on the cell proliferation and Ca^{2+} ions permeation. Colloids Surfaces B 156:388–396.

Ceccarelli G, Bloise N, Mantelli M, Gastaldi G, Fassina L, De Angelis MG, Ferrari D, Imbriani M, Visai L. 2013. A comparative analysis of the in vitro effects of pulsed electromagnetic field treatment on osteogenic differentiation of two different mesenchymal cell lineages. Biores Open Access 2:283–294.

Cormier C. 1995. Markers of bone metabolism. Curr Opin Rheumatol 7:243–248.

Corona-Gomez J, Chen X, Yang Q. 2016. Effect of nanoparticle incorporation and surface coating on mechanical properties of bone scaffolds: A brief review. J Funct Biomater 7:18–28.

Daish C, Blanchard R, Fox K, Pivonka P, Pirogova E. 2018. The application of pulsed electromagnetic fields (pEMFs) for bone fracture repair: Past and perspective findings. Ann Biomed Eng 46:525–542.

Deng X-L, Lau C-P, Lai K, Cheung K, Lau G, Li G. 2007. Cell cycle-dependent expression of potassium channels and cell proliferation in rat mesenchymal stem cells from bone marrow. Cell Prolif 40:656–670.

Edelman E, Brown L, Kost J, Taylor J, Langer R. 1984. Modulated release from polymeric drug delivery systems using oscillating mahnetic fields: In vitro and in vivo characteristics. ASAIO J 30:445–449.

Fan C, Wang D-A. 2017. Macroporous hydrogel scaffolds for three-dimensional cell culture and tissue engineering. Tissue Eng Part B Rev 23:451–461.

Ferroni L, Gardin C, Dolkart O, Salai M, Barak S, Piattelli A, Amir-Barak H, Zavan B. 2018. Pulsed electromagnetic fields increase osteogenetic commitment of MSCs via the mTOR pathway in TNF-α mediated inflammatory conditions: An in-vitro study. Sci Rep 8:5108.

Garner AL, Chen G, Chen N, Sridhara V, Kolb JF, Swanson RJ, Beebe SJ, Joshi RP, Schoenbach KH. 2007. Ultrashort electric pulse induced changes in cellular dielectric properties. Biochem Biophys Res Commun 362:139–144.

Golovin YI, Gribanovsky SL, Golovin DY, Zhigachev AO, Klyachko NL, Majouga AG, Sokolsky M, Kabanov AV. 2017. The dynamics of magnetic nanoparticles exposed to non-heating alternating magnetic field in biochemical applications: Theoretical study. J Nanopart Res 19:59.

Grant DN, Cozad MJ, Grant DA, White RA, Grant SA. 2015. In vitro electromagnetic stimulation to enhance cell proliferation in extracellular matrix constructs with and without metallic nanoparticles. J Biomed Mater Res Part B Appl Biomater 103:1532–1540.

Gupta T, Jain V, Tandon P. 1991. Comparative study of bone growth by pulsed electromagnetic fields. Med Biol Eng Comput 29:113–120.

Harris H. 1990. The human alkaline phosphatases: What we know and what we don't know. Clin Chim Acta 186:133–150.

Hasan A, Morshed M, Memic A, Hassan S, Webster TJ, Marei HE. 2018. Nanoparticles in tissue engineering: Applications, challenges and prospects. Int J Nanomed 13:5637–5655.

Hronik-Tupaj M, Rice WL, Cronin-Golomb M, Kaplan DL, Georgakoudi I. 2011. Osteoblastic differentiation and stress response of human mesenchymal stem cells exposed to alternating current electric fields. Biomed Eng Online 10:9.

Jegal S-H, Park J-H, Kim J-H, Kim T-H, Shin US, Kim T-I, Kim H-W. 2011. Functional composite nanofibers of poly (lactide–co-caprolactone) containing gelatin–apatite bone mimetic precipitate for bone regeneration. Acta Biomater 7:1609–1617.

Kanczler JM, Sura HS, Magnay J, Green D, Oreffo RO, Dobson JP, El Haj AJ. 2010. Controlled differentiation of human bone marrow stromal cells using magnetic nanoparticle technology. Tissue Eng Part A 16:3241–3250.

Kang KS, Hong JM, Kang JA, Rhie JW, Jeong YH, Cho DW. 2013. Regulation of osteogenic differentiation of human adipose-derived stem cells by controlling electromagnetic field conditions. Exp Mol Med 45:e6.

Lanyon L. 1974. Experimental support for the trajectorial theory of bone structure. J Bone Joint Surg Br 56:160–166.

Lanyon L, Baggott D. 1976. Mechanical function as an influence on the structure and form of bone. Bone Joint J 58:436–443.

Liu T-Y, Hu S-H, Liu T-Y, Liu D-M, Chen S-Y. 2006. Magnetic-sensitive behavior of intelligent ferrogels for controlled release of drug. Langmuir 22:5974–5978.

Lohmann C, Schwartz Z, Liu Y, Guerkov H, Dean D, Simon B, Boyan B. 2000. Pulsed electromagnetic field stimulation of MG63 osteoblast-like cells affects differentiation and local factor production. J Orthop Res 18:637–646.

Markov MS. 2007. Pulsed electromagnetic field therapy history, state of the art and future. Environmentalist 27:465–475.

McKibbin B. 1978. The biology of fracture healing in long bones. J Bone Joint Surg Br 60:150–162.

Meng J, Xiao B, Zhang Y, Liu J, Xue H, Lei J, Kong H, Huang Y, Jin Z, Gu N. 2013. Super-paramagnetic responsive nanofibrous scaffolds under static magnetic field enhance osteogenesis for bone repair in vivo. Sci Rep 3:2655.

Meng J, Zhang Y, Qi X, Kong H, Wang C, Xu Z, Xie S, Gu N, Xu H. 2010. Paramagnetic nanofibrous composite films enhance the osteogenic responses of pre-osteoblast cells. Nanoscale 2:2565–2569.

Misawa H, Kobayashi N, Soto-Gutierrez A, Chen Y, Yoshida A, Rivas-Carrillo JD, Navarro-Alvarez N, Tanaka K, Miki A, Takei J. 2006. PuraMatrix™ facilitates bone regeneration in bone defects of calvaria in mice. Cell Transplant 15:903–910.

Panagopoulos DJ, Karabarbounis A, Margaritis LH. 2002. Mechanism for action of electromagnetic fields on cells. Biochem Biophys Res Commun 298:95–102.

Phillips JE, Petrie TA, Creighton FP, García AJ. 2010. Human mesenchymal stem cell differentiation on self-assembled monolayers presenting different surface chemistries. Acta Biomater 6:12–20.

Polo-Corrales L, Latorre-Esteves M, Ramirez-Vick JE. 2014. Scaffold design for bone regeneration. J Nanosci Nanotechnol 14:15–56.

Polo-Corrales L, Ramirez-Vick J, Feria-Diaz JJ. 2018. Recent advances in biophysical stimulation of MSC for bone regeneration. Indian J Sci Technol 11:1–41.

Robert AW, Angulski ABB, Spangenberg L, Shigunov P, Pereira IT, Bettes PSL, Naya H, Correa A, Dallagiovanna B,

Stimamiglio MA. 2018. Gene expression analysis of human adipose tissue-derived stem cells during the initial steps of in vitro osteogenesis. Sci Rep 8:4739.
Ross CL, Siriwardane M, Almeida-Porada G, Porada CD, Brink P, Christ GJ, Harrison BS. 2015. The effect of low-frequency electromagnetic field on human bone marrow stem/progenitor cell differentiation. Stem Cell Res 15:96–108.
Sapir-Lekhovitser Y, Rotenberg MY, Jopp J, Friedman G, Polyak B, Cohen S. 2016. Magnetically actuated tissue engineered scaffold: Insights into mechanism of physical stimulation. Nanoscale 8:3386–3399.
Schwartz Z, Simon BJ, Duran MA, Barabino G, Chaudhri R, Boyan BD. 2008. Pulsed electromagnetic fields enhance BMP-2 dependent osteoblastic differentiation of human mesenchymal stem cells. J Orthop Res 26:1250–1255.
Semino C. 2008. Self-assembling peptides: From bio-inspired materials to bone regeneration. J Dent Res 87:606–616.
Sun LY, Hsieh DK, Lin PC, Chiu HT, Chiou TW. 2010. Pulsed electromagnetic fields accelerate proliferation and osteogenic gene expression in human bone marrow mesenchymal stem cells during osteogenic differentiation. Bioelectromagnetics 31:209–219.
Sun LY, Hsieh DK, Yu TC, Chiu HT, Lu SF, Luo GH, Kuo TK, Lee OK, Chiou TW. 2009. Effect of pulsed electromagnetic field on the proliferation and differentiation potential of human bone marrow mesenchymal stem cells. Bioelectromagnetics 30:251–260.
Sundelacruz S, Levin M, Kaplan DL. 2008. Membrane potential controls adipogenic and osteogenic differentiation of mesenchymal stem cells. PLoS One 3:e3737.
Sundelacruz S, Levin M, Kaplan DL. 2009. Role of membrane potential in the regulation of cell proliferation and differentiation. Stem Cell Rev Rep 5:231–246.
Voog J, Jones DL. 2010. Stem cells and the niche: A dynamic duo. Cell Stem Cell 6:103–115.
Wang H, Li Y, Zuo Y, Li J, Ma S, Cheng L. 2007. Biocompatibility and osteogenesis of biomimetic nano-hydroxyapatite/polyamide composite scaffolds for bone tissue engineering. Biomaterials 28:3338–3348.
Wei Y, Zhang X, Song Y, Han B, Hu X, Wang X, Lin Y, Deng X. 2011. Magnetic biodegradable Fe_3O_4/CS/PVA nanofibrous membranes for bone regeneration. Biomed Mater 6:055008.
Woo S, Kuei SC, Amiel D, Gomez M, Hayes W, White F, Akeson W. 1981. The effect of prolonged physical training on the properties of long bone: A study of Wolff's law. J Bone Joint Surg Am 63:780–787.
Wu Y, Jiang W, Wen X, He B, Zeng X, Wang G, Gu Z. 2010. A novel calcium phosphate ceramic–magnetic nanoparticle composite as a potential bone substitute. Biomed Mater 5:015001.
Xu H-Y, Gu N. 2014. Magnetic responsive scaffolds and magnetic fields in bone repair and regeneration. Front Mater Sci 8:20–31.
Yelin E, Weinstein S, King T. 2016. The burden of musculoskeletal diseases in the United States. Semin Arthritis Rheum 46:259–260.
Yoshimura K, Sokabe M. 2010. Mechanosensitivity of ion channels based on protein–lipid interactions. J R Soc Interface 7:S307–S320.
Yun H-M, Lee E-S, Kim M-J, Kim J-J, Lee J-H, Lee H-H, Park K-R, Yi J-K, Kim H-W, Kim E-C. 2015. Magnetic nanocomposite scaffold-induced stimulation of migration and odontogenesis of human dental pulp cells through integrin signaling pathways. PLoS One 10:e0138614.
Zeng XB, Hu H, Xie LQ, Lan F, Jiang W, Wu Y, Gu ZW. 2012. Magnetic responsive hydroxyapatite composite scaffolds construction for bone defect reparation. Int J Nanomedicine 7:3365.
Zhang S. 2004. Beyond the Petri dish. Nature Biotechnol 22:151–152.
Zhao D, Wu H, Li F, Li R, Tao C. 2008. Electromagnetic field change the expression of osteogenesis genes in murine bone marrow mesenchymal stem cells. J Huazhong Univ Sci Technolog Med Sci 28:152–155.
Zhao X, Kim J, Cezar CA, Huebsch N, Lee K, Bouhadir K, Mooney DJ. 2011. Active scaffolds for on-demand drug and cell delivery. Proc Natl Acad Sci 108:67–72.
Zhong C, Zhang X, Xu Z, He R. 2012. Effects of low-intensity electromagnetic fields on the proliferation and differentiation of cultured mouse bone marrow stromal cells. Phys Ther 92:1208–1219.
Zhu Y, Yang Q, Yang M, Zhan X, Lan F, He J, Gu Z, Wu Y. 2017. Protein corona of magnetic hydroxyapatite scaffold improves cell proliferation via activation of mitogen-activated protein kinase signaling pathway. ACS Nano 11:3690–3704.

SUPPORTING INFORMATION

Additional supporting information may be found online in the Supporting Information section at the end of the article.